Applied Catalysis B: Environmental 123–124 (2012) 398–404

Contents lists available at SciVerse ScienceDirect

Applied Catalysis B: Environmental

journal homepage: www.elsevier.com/locate/apcatb

WO_3 nanocrystals with tunable percentage of (0 0 1)-facet exposure

Dieqing Zhang [a], Songling Wang [a], Jian Zhu [a], Hexing Li [a,*], Yunfeng Lu [b,**]

[a] Key laboratory of resource chemistry of ministry of education and Shanghai Key laboratory of rare earth functional materials, Shanghai Normal University, Shanghai 200234, China
[b] Chemical & Biomolecular Engineering Department, University of California, Los Angeles, CA 90095, USA

ARTICLE INFO

Article history:
Received 8 February 2012
Received in revised form 10 April 2012
Accepted 30 April 2012
Available online 5 May 2012

Keywords:
WO_3
High-energy
Facets
Photocatalysis

ABSTRACT

Orthorhombic WO_3 nanocrystals with tunable percentage of (0 0 1)-facet exposure were synthesized by hydrothermal reaction using BF_4^- as the guiding agent. The preferable exposure of the high-energy (0 0 1) facets endows the nanocrystals with significantly enhanced photocatalytic activity as probed by photodegradation of Rhodamine B and the electron spin resonance techniques.

1. Introduction

Photocatalysts hold great promises for broad range of applications [1]; their performance is often governed by the intrinsic optoelectronic and crystallographic characteristics. Making photocatalytically active nanocrystals with preferable exposure of their active facets has become as an effective route towards better photocatalysts. To achieve the preferable exposure of the active facets, ions and molecules were often used as the guiding agents during their synthesis, which led to the formation of large varieties of photocatalysts with crystallographic control. Typical examples include the nanocrystals of anatase TiO_2 [2] and $BiVO_4$ [3] with preferable (0 0 1) exposure, Ag_3PO_4 with preferable (1 1 0) exposure [4,5], and ZnO with preferable (0 0 0 1) exposure [6]. However, except $BiVO_4$ and Ag_3PO_4 nanocrystals, most of the crystals possess bang gaps higher than those of the visible light, and their photocatalytic reactions have to be conducted under ultraviolet light irradiation. Developing photocatalytic nanocrystals with preferable exposure of the high-energy facets and with visible-light-driven catalytic activity has been an attractive but challenging topic.

In this context, tungsten oxide (WO_3) with a narrow energy band gap ~2.3 eV holds great potential for visible-light-driven photocatalytic applications [7]. However, WO_3 commonly exists in the monoclinic form with extremely low photocatalytic activity. Using BF_4^- as the guiding agent, we report herein the synthesis of orthorhombic WO_3 nanocrystals with preferable exposure of the (0 0 1) facets, the high-energy facets.

2. Experimental

2.1. Preparation

In a typical synthesis, 2.33 g ammonium tungstate hydrate (Sinopharm chemical reagent Co., Ltd.) was added into 20 mL fluoroboric acid (50% solution in water, J&K Chemical Ltd.) while stirring. After 1 h stirring, the yellow solution was transferred into a 50 mL Teflon-lined stainless autoclave. The autoclave was heated to 160 °C and maintained for 24 h. The solid product, denoted as WO_3-1, was collected and washed thoroughly with deionized water, followed by drying at 100 °C in air. WO_3-2 and WO_3-3 were synthesized in the similar way to the WO_3-1 by using 25% or 12.5% HBF_4, respectively. The WO_3-C refers to the commercially available WO_3 and used without further treatment. WO_3-1-350 and WO_3-1-400 were prepared by calcining WO_3-1 in air at 350 °C and 400 °C, respectively. WO_3-4 was prepared by immersing WO_3-1-400 in 25% HBF_4 aqueous solution for 24 h. WO_3-5 was synthesized in the same method as that used for WO_3-1 by using $Na_2WO_4{\cdot}2H_2O$ instead of $(NH_4)_2WO_4$. Briefly, 1.0 g $Na_2WO_4{\cdot}2H_2O$ was added into 80 mL 50% HBF_4 aqueous solution while stirring. After 1 h stirring, the yellow solution was transferred into a 100 mL Teflon-lined stainless autoclave for 24 h hydrothermal treatment at 160 °C. The solid product was collected and washed with DI water thoroughly, followed by drying at 100 °C in air.

* Corresponding author. Fax: +86 021 64322272.
** Corresponding author.
E-mail addresses: hexing-li@shnu.edu.cn (H. Li), luucla@ucla.edu (Y. Lu).

0926-3373/$ – see front matter © 2012 Elsevier B.V. All rights reserved.
http://dx.doi.org/10.1016/j.apcatb.2012.04.049

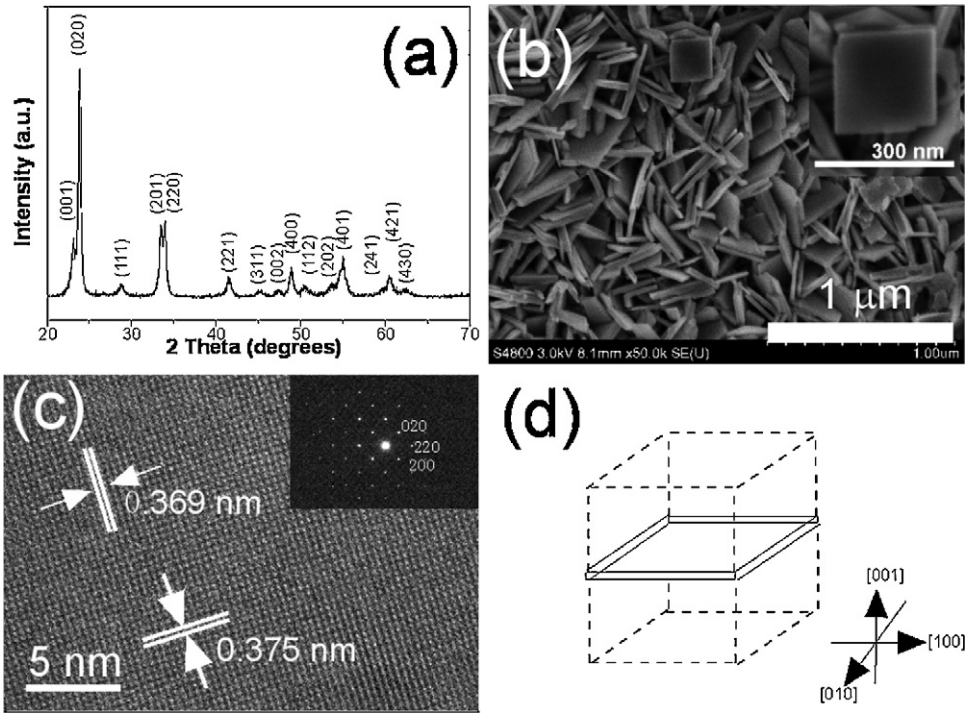

Fig. 1. XRD pattern (a), FESEM image (b), higher-magnification FESEM image (b, inset), HRTEM image (c), SAED pattern (c, inset) and a schematic illustration of the crystallographic orientation of the WO_3-1 nanocrystals.

2.2. Characterization

X-ray diffraction (XRD) patterns were recorded using a D/MAX-2000 diffractometer with high-intensity Cu Kα irradiation (λ = 1.5406 Å). Transmission electron microscopy (TEM) and field emission scanning electron microscopy (FESEM) images were collected on a JEM-2100 microscope and JEOL JSM-6380LV microscope, respectively. X-ray photoelectron spectroscopy (XPS) measurement was conducted on a PerkinElmer PHI 5000C XPS system with a monochromatic Al Kα source and a charge neutralizer. All the binding energy values were calibrated by using C 1S = 284.6 eV as a reference. The photoluminescent (PL) spectra were recorded on a Varian Cary-Eclipse 500 with an excitation wavelength of 370 nm.

2.3. Activity testing

The photocatalytic degradation of Rhodamine B (RhB) was carried out in an aqueous solution at ambient temperature. Briefly, in a 100 mL beaker, 0.050 g WO_3 single crystal photocatalyst was suspended in 50 mL aqueous solution containing 5 ppm RhB. The aqueous suspension was stirred for 1 h to reach an adsorption/desorption equilibrium. The photocatalytic degradation of RhB was initiated by irradiating the reaction mixture with a commercial 500 W Xe lamp surrounded. A piece of Pyrex glass was used to cut off the UV lights below 420 nm. The light source was located at 18 cm from the reaction solution. After 4 h reaction, the photodegradation was monitored by measuring the absorbance of the solution of 550 nm. Preliminary tests demonstrated a good linear relationship between the light absorbance and the RhB concentration. Only less than 2.0% RhB decomposed after reaction for 4 h in the absence of either the photocatalyst or the light irradiation and, thus, could be neglected in comparison with the RhB degraded via photocatalysis.

2.4. Surface energy calculation

The DFT calculations were carried out with a VASP package using plane wave basis sets. The exchange-correlation function used is the local-density-approximation with generalized gradient correction, known as GGA-PW91. The surfaces were modeled by six-layer p (1×1) slabs in which the middle two layers were fixed at their bulk geometry and the vacuum separation between the slabs was 15 Å. The surface energy of the clean WO_3 surfaces is defined as:

$$E_{surf} = \frac{(E_{slab} - n \times E_{bulk})}{(2 \times A)}$$

where E_{slab} is the total energy of the relaxed slab, E_{bulk} is the total energy of the bulk, n is the number of the bulk unit cells in the supercell to model the surface, and A is the surface area.

3. Results and discussion

3.1. Photocatalysts characterization

Fig. 1a shows X-ray diffraction (XRD) pattern of the nanocrystals exhibiting an orthorhombic structure (a = 7.384 nm, b = 7.512 nm, c = 3.846 nm, JCPDS No.20-1324). Field emission scanning electron microscopy (FESEM) image reveals uniform nanosheet morphology with 200–300 nm in width and 15–20 nm in thickness (Fig. 1b). High-resolution transmission electron microscopy (HRTEM) image indicates a fringe spacing of 0.369 nm and 0.375 nm, which is consistent with the (2 0 0) and (0 2 0) lattice planes of orthorhombic WO_3, respectively (Fig. 1c). The inset in Fig. 1c shows a representative selected-area electron diffraction (SAED) pattern taken along the direction perpendicular to the nanosheets. The resulted diffraction spots indexed as the (2 0 0), (0 2 0) and (2 2 0) reflections suggest the preferable exposure of the (0 0 1) facets (Fig. 1d). Based on the dimension and geometry of the nanosheets, it is estimated that around 91% of the crystal surfaces are the (0 0 1) facets

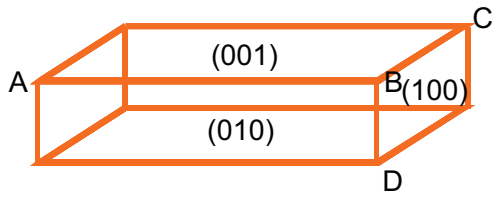

$S_{001}=2AB*BC$

$S_{010}=2AB*BD$

$S_{100}=2BC*BD$

$S_{001}\%=S_{001}/(S_{001}+S_{010}+S_{100})$
$=BC/(BC+BD+BC*BD/AB)$

Fig. 2. Model of orthorhombic WO_3 single crystal and the process for calculating the percentage of exposed (0 0 1) facet.

(Fig. 2), which is dramatically higher in comparison with those of ZnO (50%)[6] and TiO_2 (47%) nanocrystals [8].

Generally, normal growth of an orthorhombic crystal along its [0 0 1], [1 0 0] and [0 1 0] axes leads to crystals with non-preferable facet exposure (see the supporting information). We believe that the preferable (0 0 1)-facet exposure is attributed from preferable adsorption of BF_4^- ions onto the (0 0 1) facets, the facets with higher surface energy than those of (1 0 0) and (0 1 0) facets, during their crystal growth. The preferable BF_4^- adsorption inhibits the crystal growth along the [0 0 1] axis direction, resulting in the formation of nanosheet-shape nanocrystals with increased exposure of the (0 0 1) facets (Fig. 3).

To confirm the (0 0 1) facets do possess higher energy than those of the (1 0 0) and (0 1 0) facets, density functional theory (DFT) calculations were applied and their atomic structure and surface energy were also compared (see Support Information for details). Fig. 4 shows theoretical models illustrating the crystal structure and two-dimensional (2D) atom arrangements of the (0 0 1), (1 0 0) and (0 1 0) facets in an orthorhombic WO_3 crystal, in which the purple planes represent the (0 0 1), (1 0 0) and (0 1 0) facets. Obviously, the arrangement of the W and O atoms on the (0 0 1) facets are different from those on either (1 0 0) or (0 1 0) facets and are more closely spaced on the (0 0 1) facets. The atom arrangement observed in the (0 0 1) facets might result in higher density of corners and edges, which often leads to higher catalytic activity [2,9]. The

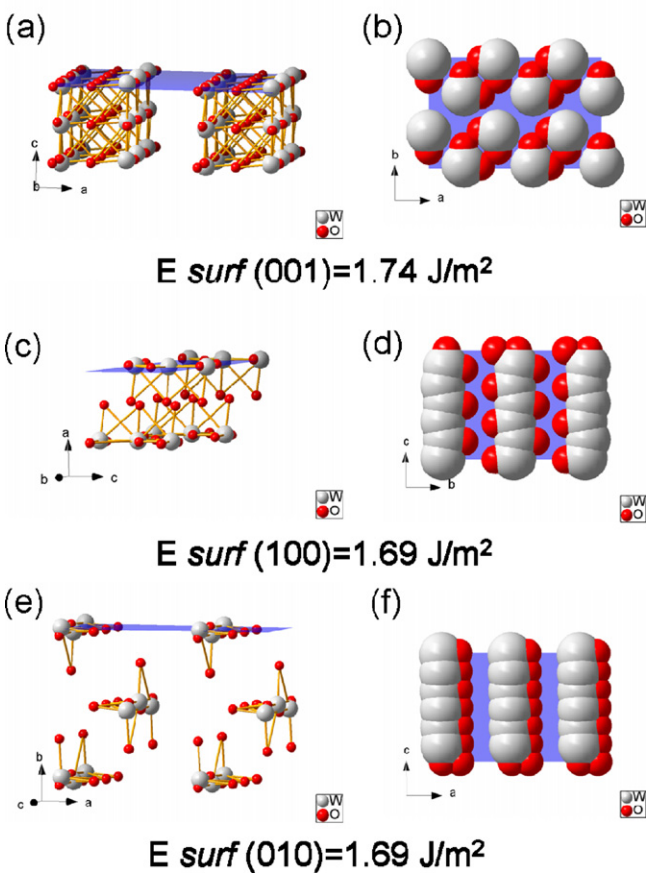

Fig. 4. Schematic drawing of the crystal structure and 2D atom arrangement on the (0 0 1) (a, b), (1 0 0) (c, d) and (0 1 0) facets (e, f) of an orthorhombic WO_3 crystal. The purple planes are the (0 0 1), (1 0 0) and (0 1 0) facets.

surface energy of the (0 0 1) facets is estimated to be ~1.74 J/m^2, which is higher than that of the (1 0 0) facets (~1.69 J/m^2) or (0 1 0) facets (~1.69 J/m^2). These studies thermodynamically confirm the tendency of the BF_4^- ions preferably adsorbing onto the (0 0 1) facets, as well as a feasibility of making WO_3 nanocrystals with preferable (0 0 1) facet exposure and enhanced catalytic activity.

The preferable adsorption of BF_4^- ions onto the crystals was confirmed by X-ray photoelectron spectroscopy (XPS) spectra

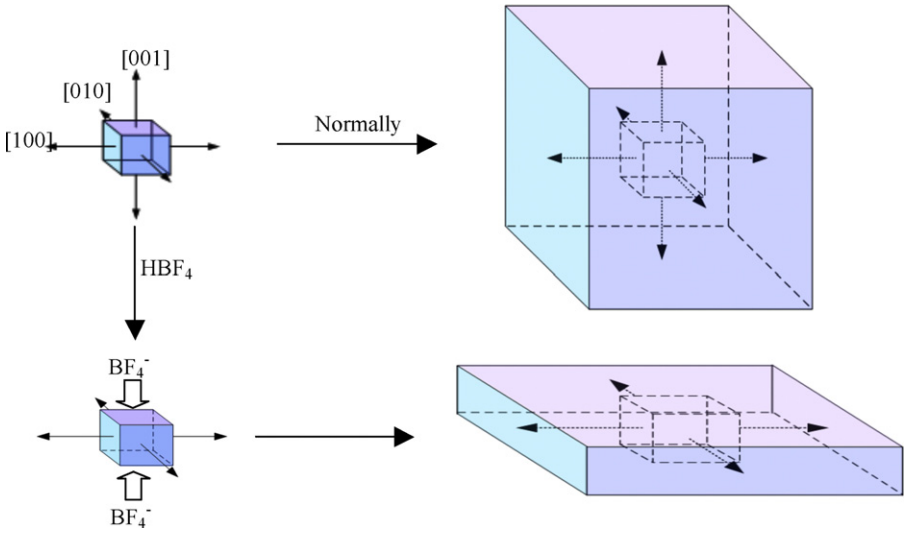

Fig. 3. Schematic illustration of the growth of the WO_3 orthorhombic crystal.

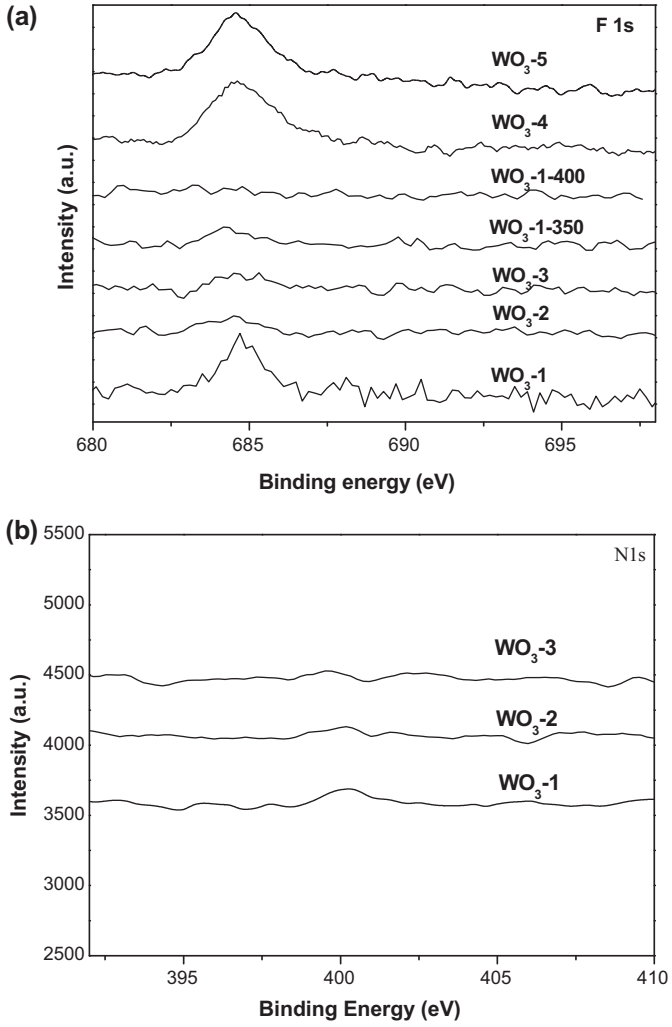

Fig. 5. F 1s (a) and N 1s (b) XPS spectra of different WO_3 samples.

studies. Fig. 5 shows XPS spectra of WO_3-1. The presence of F 1s peak at 684.6 eV clearly indicates the presence of BF_4^- ions; while no N 1s signal is observed indicating the absence or insignificant presence of NH_4^+ ions on the nanocrystals. The presence of BF_4^- ions on the nanocrystals is consistent with the isoelectric point (IEP) of WO_3 (~0.2–0.5), which leads to a positively surface charge in the acidic synthesis-media used in this work (pH < 1). Since BF_4^- ions are highly electronegative, they may preferably adsorb on the high-energy (0 0 1) facets than the low-energy (0 1 0) and (1 0 0) facets. It is also worthy mentioning that calcinating WO_3-1 at 400 °C effectively removed the BF_4^- ions; while exposing the calcined crystals to a HBF_4 solution allowed the re-adsorption of BF_4^- ions onto the crystal (Fig. 5), indicating that the BF_4^- ions were indeed adsorbed on the nanocrystals.

Table 1
Surface area, F/W ratios, percentage of the (0 0 1) facet exposure vs. the total surface of the nanocrystals, and photocatalytic activity of the WO_3 nanocrystals probed by photodegradation of Rhodamine B.

Sample	S_{BET} (m^2/g)	F/W (%)	Percentage of (0 0 1) facets (%)	Photocatalytic activity (%)
WO_3-1	15	13	91	87
WO_3-2	8	8	69	62
WO_3-3	4	5	41	32
WO_3-C	10	0	0	19

Such a BF_4^--ion-guiding growth mechanism enables the synthesis of WO_3 nanocrystals with tunable percentage of their (0 0 1)-facet exposure by simply adjusting the BF_4^- ion concentration. To demonstrate this concept, Fig. 6 shows SEM images of WO_3 nanocrystals prepared from the reaction media containing 25 wt% and 12.5 wt% HBF_4, which are denoted as (a) WO_3-2 and (b) WO_3-3, respectively. Consistently, XPS results suggested that the F/W ratios (calculated based on the area ratio of the principle peaks of F 1s and W 4f) decrease with reducing HBF_4 concentration (Table 1). As expected, these nanocrystals show width (~200–300 nm) similar to those of WO_3-1; however, the thickness of the nanocrystals increases from ~16 nm for WO_3-1 to ~70 nm for WO_3-2 and to ~110 nm for WO_3-3. The increasing crystal thickness corresponds to the decreasing percentage of the (0 0 1) facets from 91% to 69% and 41%, respectively. Table 1 also lists the surface areas of these nanocrystals showing a systematically decreasing surface area with the decreasing percentage of the (0 0 1) facet exposure. Overall, these studies clearly confirm a feasibility of tuning the percentage of active-facet exposure by guiding-ion concentration.

3.2. Photocatalytic activity

The ability to synthesize WO_3 nanocrystals with tunable percentage of active-facet exposure provides an effective route to tune their photocatalytic activity. In this work, photocatalytic activities of the WO_3 nanocrystals were probed by visible-light-induced photodegradation of Rhodamine B (RhB) (see Supporting Information for details). Commercial orthorhombic WO_3 crystals (denoted as WO_3-C) with a surface area similar to those of the nanocrystals synthesized (Table 1) but without preferable (0 0 1) exposure were used as a reference (see XRD and TEM in Fig. 7). It was found that the degradation is a first order reaction with the respect to RhB concentration (Fig. 8). Table 1 lists the yields of the degradation reaction after 4 h reaction. Clearly, WO_3-1 exhibits the highest activity that is near 5 times of that of WO_3-C. Considering WO_3-1 and WO_3-C

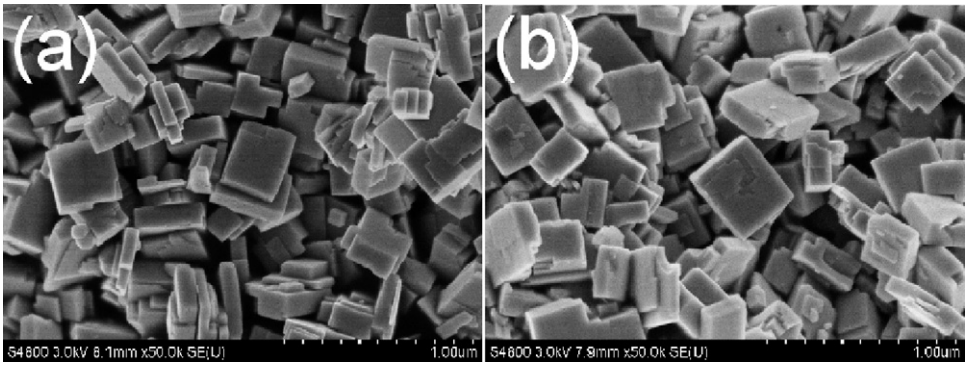

Fig. 6. FESEM images of (a) WO_3-2 and (b) WO_3-3 nanocrystals.

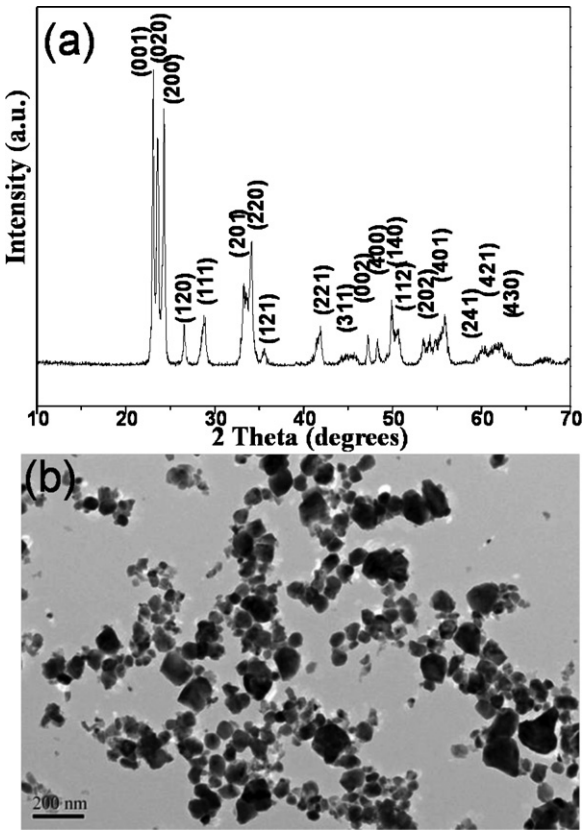

Fig. 7. XRD pattern (a) and TEM image (b) of WO_3-C.

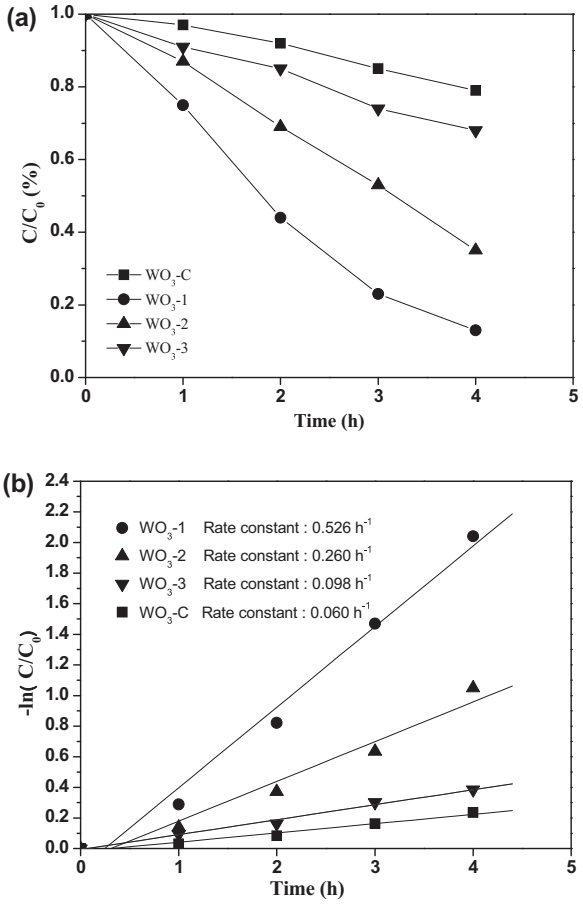

Fig. 8. (a) Plots of the decrease in the concentration of RhB vs. irradiation time of visible light irradiation ($\lambda > 420$ nm) in the presence of different WO_3 photocatalysts. (b) Dependence of $-\ln(C/C_0)$ on the irradiation time.

possess similar surface area, such dramatically enhanced photocatalytic activity is attributed to the preferable exposure of the highly active (001) facets. Consistently, with decreasing percentage the (0 0 1) facet exposure, WO_3-2 and WO_3-3 show a decreased activity of 62% and 32%, respectively. Nevertheless, such activity is still two to three folds enhancement over WO_3-C, further confirming our hypothesis.

Note that active oxygen species (e.g., $^{\bullet}OH$ and $^{\bullet}O_2^-$) are often generated in photocatalytic reactions through the reactions of photo-induced charge carriers with adsorbed hydroxyl groups or O_2 [10]. We suspected that such active species also attribute to the visible-light-driven photodegradation of RhB observed here. Indeed, it was found that removing the oxygen molecules from the reaction media by purging the media with nitrogen led to an abrupt decrease of RhB-degradation rate (Fig. 9). This can be explained as the reduced oxygen concentration inhibiting the formation of $^{\bullet}O_2^-$ active species. Similarly, RhB degradation rate decreased abruptly when isopropanol (*i*-PrOH), a scavenger for $^{\bullet}OH$ radicals, was added into the reaction solution (Fig. 9). These findings confirm the photodegradation of RhB involving these active species.

To confirm this mechanism, electron spin resonance (ESR) spin-trapping studies were conducted using 5,5-dimethyl-1-pyrroline-N-oxide (DMPO) as the spin-trap reagent. As shown in Fig. 10, typical ESR spectra of the DMPO-$^{\bullet}OH$ adducts with a quartet signal (intensity ratio of 1:2:2:1) were clearly observed after the irradiation of WO_3-1 dispersed in water for 3 min. Meanwhile, the ESR spectra of DMPO-$^{\bullet}O_2^-$ adducts were also observed after the irradiation of WO_3-1 dispersed in benzene alcohol for the same time. In comparison with the corresponding ESR spectra obtained from WO_3-C (Fig. 11), WO_3-1 exhibits much intense signals for the DMPO-$^{\bullet}OH$ and DMPO-$^{\bullet}O_2^-$ adducts after the same irradiation time. This comparison clearly indicates that WO_3-1 with preferably exposed (0 0 1) facets does generate more $^{\bullet}OH$ and $^{\bullet}O_2^-$ active species under visible-light irradiation, which leads to enhanced photocatalytic activity.

There are two possible reasons accounting for the more effective generation of $^{\bullet}OH$ and $^{\bullet}O_2^-$ active species by WO_3-1. Firstly, WO_3-1 with preferable (0 0 1) facet exposure could be more easily activated by visible light to produce photo-induced charge carriers, which could react with adsorbed hydroxyl groups and O_2 and

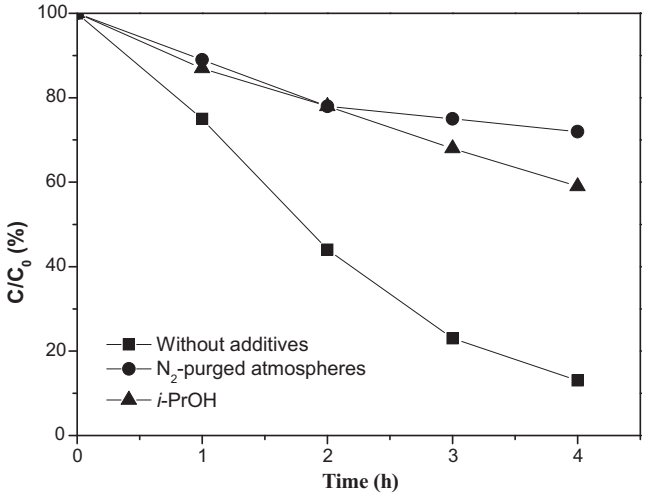

Fig. 9. Effects of N_2-purged atmospheres and *i*-PrOH on degradation rate of RhB in aqueous WO_3 suspension.

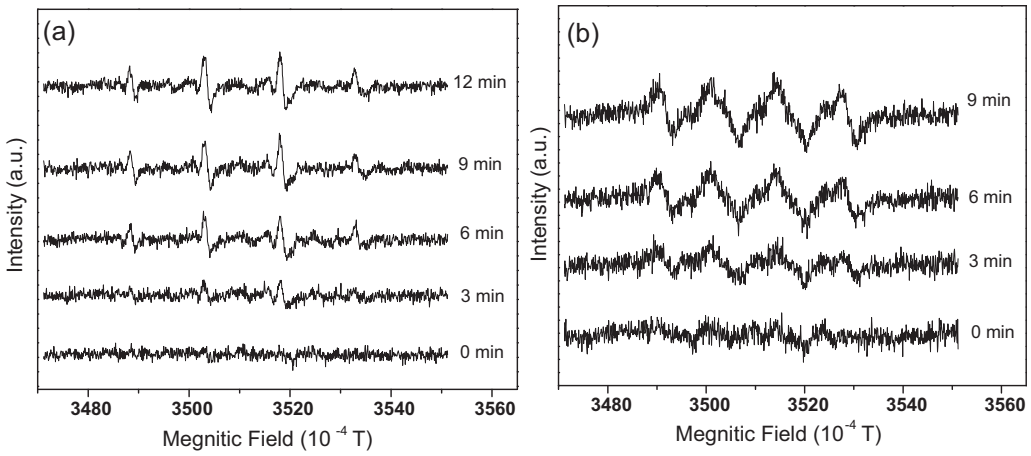

Fig. 10. (a) ESR spectra of DMPO-•OH adducts after irradiation of WO_3-1 dispersed in H_2O and (b) ESR spectra of DMPO-•O_2- adducts after irradiation of WO_3-1 dispersed in benzyl alcohol after irradiation using visible light for different time.

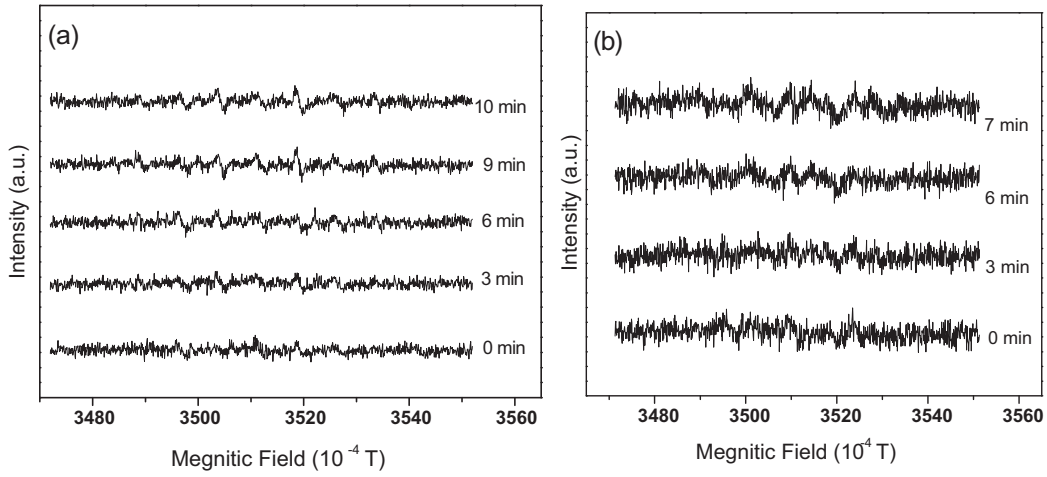

Fig. 11. (a) ESR spectra of DMPO-•OH adducts after irradiation of WO_3-C dispersed in H_2O and (b) ESR spectra of DMPO-•O_2^- adducts after irradiation of WO_3-C dispersed in benzyl alcohol.

yield more •OH and •O_2^- active species. This could be confirmed by the increasing signal intensities of DMPO-•OH and DMPO-•O_2^- adducts for WO_3-1 with increasing irradiation time (Fig. 10). While the signal intensities of both DMPO-•OH and DMPO-•O_2^- adducts for WO_3-C remained almost constant (Fig. 11). Secondly, photoluminescent spectra of WO_3-1 displayed a weaker dual-frequency peak around 740 nm than that of WO_3-C (Fig. 12), implying that the nanocrystals with preferably exposed (0 0 1) facets experience less recombination of the photo-induced electrons and holes [11], leading to further enhanced activity and efficiency.

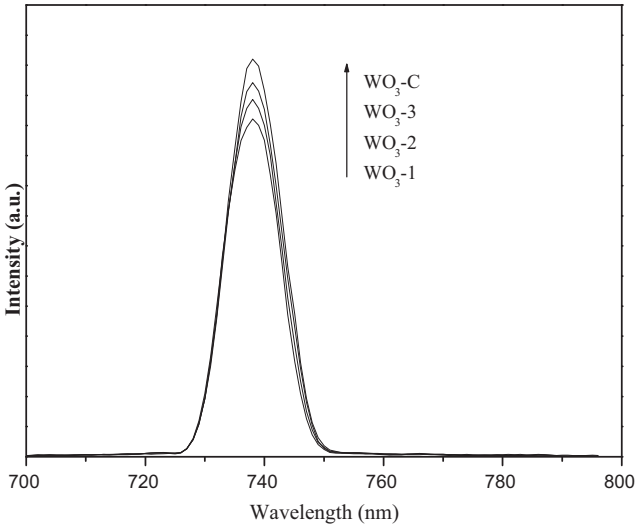

Fig. 12. Photoluminescent (PL) spectra of different WO_3 samples.

4. Conclusions

In conclusion, we have synthesized orthorhombic WO_3 single crystals with tunable percentage of (0 0 1) facet exposure using BF_4^- as the guiding agent. The preferable exposure of the highly active (0 0 1) facets endows the nanocrystals with significantly enhanced photocatalytic activity, which can be attributed to the more effective production of active oxygen species and reduced recombination of photo-induced electrons and holes. This work provides an effective route towards the synthesis of photocatalytic crystals with better performance.

Acknowledgments

This work was supported by the National Natural Science Foundation of China (21007040, 21047009, 20825724), the Research Fund for the Doctoral Program of Higher Education (20103127120005), the Innovation Program of Shanghai Municipal

Education Commission (12YZ079), the Foundation of Shanghai Government (11PJ1407500, 10160503200, 11ZR1426300, 07dz22303, S30406) and by a Scheme administrated by Shanghai Normal University (SK201104). We also thank Dr. Liyan Xie from Research Institute of Photocatalysis, Fuzhou University for the ESR measurements.

References

[1] D. Ravelli, D. Dondi, M. Fagnoni, A. Albini, Chemical Society Reviews 38 (2009) 1999–2011.
[2] G. Liu, J.C. Yu, G.Q. Lu, H.M. Cheng, Chemical Communications (2011) 6763–6783.
[3] G.C. Xi, J.H. Ye, Chemical Communications (2010) 1893–1895.
[4] Z. Yi, J. Ye, N. Kikugawa, T. Kako, S. Ouyang, H. Stuart-Williams, H. Yang, J. Cao, W. Luo, Z. Li, Y. Liu, R. Withers, Nature Materials 9 (2010) 559–564.
[5] Y.P. Bi, S.X. Ouyang, N. Umezawa, J.Y. Cao, J.H. Ye, Journal of the American Chemical Society 133 (2011) 6490–6492.
[6] S. He, S.T. Zhang, J. Lu, Y.F. Zhao, J. Ma, M. Wei, D.G. Evans, X. Duan, Chemical Communications (2011) 10797–10799.
[7] R. Abe, H. Takami, N. Murakami, B. Ohtani, Journal of the American Chemical Society 130 (2008) 7780–7781.
[8] H.G. Yang, C.H. Sun, S.Z. Qiao, J. Zou, G. Liu, S.C. Smith, H.M. Cheng, G.Q. Lu, Nature 453 (2008) 638–641.
[9] N. Tian, Z.Y. Zhou, S.G. Sun, Y. Ding, Z.L. Wang, Science 316 (2007) 732–735.
[10] A.L. Linsebigler, G.Q. Lu, J.T. Yates, Chemical Reviews 95 (1995) 735–758.
[11] H.X. Li, G.S. Li, J. Zhu, Y. Wan, Journal of Molecular Catalysis A: Chemical 226 (2005) 93–100.